International Journal of GEOMATE, May 2023, Vol. 24, Issue 105, pp.93-100
ISSN: 2186-2982 (P), 2186-2990 (O), Japan, DOI: https://doi.org/10.21660/2023.105.s8572
Geotechnique, Construction Materials and Environment

# ANALYTICAL STUDY OF THE STRENGTH CHARACTERISTICS OF COMPACTED SOIL

Kazuki Naito[1], *Shin-ichi Kanazawa[2], Kira Iida[1] amd Daiki Yamashita[1]

[1] Environmental Science and Technology, Master's Program Graduate School of Science and Technology Niigata University, Japan; [2,] Civil Engineering Program, Faculty of Engineering, Niigata University, Japan

*Corresponding Author, Received:15 March 2022, Revised: 02 Feb. 2023, Accepted: 12 March 2023

**ABSTRACT:** In recent years, many cases of river embankments and levees collapsing due to sudden torrential rains and earthquakes have been reported. The mechanism of compaction and collapse based on the mechanics of unsaturated soil is important to establish a quality evaluation method for embankment structures in consideration of performance design. Therefore, in this study, compaction behavior considering soil materials was analyzed using the soil-water-air coupled finite element analysis program (DACSAR-MP). The obtained compacted specimens of silt-mixed sand were then subjected to flooding analysis and constant volume shear analysis to determine the strength properties from the numerical analysis. The results of the analysis showed that over compaction was confirmed by considering air dissolution, and that suction stress had a significant effect on shear strength, resulting in a significant reduction in strength on the wet side. In conclusion, the analysis showed that construction on the dry side is safer and stronger in construction using D values.

*Keywords: Compaction curve, Unsaturated soils, Water characteristic curve*

## 1. INTRODUCTION

Many cases of riverbank and embankment failure have been reported in recent years due to sudden heavy rains, typhoon torrential rains, and earthquakes. Originally, soil structures are composed of compacted soil to improve stability and deformation characteristics. In the field, D-value is the standard for construction of soil structures using compacted soil as material, such as embankments, and there are various execution management methods for soil structures so that the appropriate one can be selected depending on the type of soil used and execution method. However, the mechanisms of the strength development of compacted soil in the field and its relationship with the strength of the soil and its relationship with the strength and collapse of soil structures in response to such natural hazards have not been fully elucidated. Current construction guidelines do not prepare mangers for the maintenance of embankments subjected to recent torrential rains and earthquakes. In the field, soil structures are subjected to climatic conditions such as repeated dry and wet weather. The influence of unsaturated soil behavior cannot be ignored. In the future, there will be a shift from the conventional specification design method to performance design, which is a design method that verifies the required performance. In order to establish a quality evaluation method for soil structures considering performance design, it is important to propose an index for evaluating compacted soil by clarifying the relationship between compaction mechanism and strength of embankment structures based on unsaturated soil mechanics, as well as the mechanism leading to collapse.

In this study, using the coupled soil/water/air finite element analysis program (DACSAR-MP) [1][2], the mechanical behavior of unsaturated soil due to compaction is considered as a three-layer coupled problem, and the mechanical interpretation of compaction behavior considering the difference of soil materials is analytically investigated. Subsequently, the obtained compacted specimens are subjected to flooding analysis and shear analysis to understand the strength properties from the numerical analysis.

## 2. RESEARCH SIGNIFICANCE

The mechanism of strength development and the relationship between strength and strength of compacted soil in the field have not been fully elucidated. In addition, in the accompanying past research, there have been many studies that assumed saturated soil, but none that assumed unsaturated soil. Therefore, in this paper, the studies conducted assuming saturated soil, as shown in the previous studies, were analyzed assuming unsaturated soil by dissolving air in the soil. The results obtained by the three types of analysis were closer to the real phenomena, and the usefulness of this analysis code as a tool for future analysis was demonstrated.

## 3. ANALYSIS METHOD

In this study, we use the air-dissolved unsaturated soil / water / air coupled finite analysis code

"DACSAR-MP" [1][2]. The unsaturated soil elastic-plastic composition model, the water retention curve model, and the finite element formulation in this analysis code are described below.

### 3.1 The Unsaturated Soil Elastic-plastic Composition Model

So far, several unsaturated soil composition models have been proposed, but the elastic-plastic composition model of unsaturated soil proposed by Ohno et al [3] is used in this analysis code. Ohno et al [3] propose a model in which the effective saturation is used as a state agent to express the rigidity, with reference to the model given the definition of effective stress considering the water content of Karube et al [4]. The effective stress is given by the following equations, Equation (1) shows the effective stress, Equation (2) shows the basic stress tensor and attractive stress, and Equation (3) shows the attractive force.

$$\boldsymbol{\sigma}' = \boldsymbol{\sigma}^N + p_s \mathbf{1} \tag{1}$$

$$\boldsymbol{\sigma}^N = \boldsymbol{\sigma} - p_a \mathbf{1}, \ \ p_s = sS_e \tag{2}$$

$$s = p_a - p_w, \ S_e = \frac{S_r - S_{rc}}{1 - S_{rc}} \tag{3}$$

Here, $\boldsymbol{\sigma}'$ is the effective stress tensor; $\boldsymbol{\sigma}^N$ is the base stress tensor; $\boldsymbol{\sigma}$ is the total stress tensor; $\mathbf{1}$ is the second order unit tensor; $p_a$ is the pore air pressure; $p_s$ is the suction stress; $s$ is the suction; $p_w$ is the pore water pressure; $S_e$ is the effective degree of saturation; and $S_{rc}$ is the degree of saturation at $s \to \infty$.

Furthermore, in this study, the EC model of Ohno et al [5], which has no singular point on the yield surface (e.g., pre-consolidation stress at saturation), was incorporated into the analysis code to avoid shifting to a singular point that cannot be differentiated in numerical calculation. The EC model is an elastic-plastic composition model that expresses the soil's contractility characteristics as an exponential function. Ohno et al [5] derived the yield function of unsaturated soil as follows.

$$f\left(\boldsymbol{\sigma}', \zeta, \varepsilon_v^p\right) = MD \ln \frac{p'}{\zeta p'_{sat}} + \frac{MD}{n_E}\left(\frac{q}{Mp'}\right)^{n_E} - \varepsilon_v^p = 0 \tag{4}$$

Here, $p'_{sat}$ is the yield stress at saturation; $p'$ is mean effective principal stress; $q$ is axial stress; $M$ is $q/p'$ in the limit state; $D$ is the dilatancy coefficient; $\varepsilon_v^p$ is the plastic volume strain; and $n_E$ is the shape parameter.

In addition, the increase in consolidation yield stress due to desaturation is expressed in the form of $\zeta$ times the consolidation yield stress $p'_{sat}$ in the saturated state. $\zeta$ is a function of the effective saturation and can be expressed as the following equation.

$$\zeta = \exp\left[(1 - S_e)^b \ln a\right] \tag{5}$$

Where, $b$ is parameter to adjust the spacing of the is saturation lines on plane $e - \ln p'$, and $a$ is a parameter that determines the multiplication factor of the consolidation yield stress when the increase in rigidity due to desaturation is maximum. In particular, $a$ is often treated as a fitting parameter.

Substituting $n_E = 1.0$ into Equation (4) gives the following equation.

$$f\left(\boldsymbol{\sigma}', \zeta, \varepsilon_v^p\right) = MD \ln \frac{p'}{\zeta p'_{sat}} + D\eta - \varepsilon_v^p = 0 \quad \left(\eta = \frac{q}{p'}\right) \tag{6}$$

From Equations (3) and (5), it is shown that Equation (6) is the original Cam-Clay model [6] because it holds $\zeta = 1$ in the saturated state ($S_e = 1$).

Fig. 1[3] shows a conceptual diagram of the yield surface of unsaturated soil shown by the $S_e$ - Hardening model, and Fig.2[5] shows the yield surface of the EC model proposed by Ohno et al [4]. This shows that the larger $n_E$ is, the more the singular point is eliminated and becomes differentiable. In the case of $n_E = 2.0$, this is similar to the modified Cam-Clay model [8]. In this analysis code, the EC model is used as an isotropic model.

ratio $w_C$ at $s \to \infty$, and if the influence of the gap is ignored, the saturation degree that converges at $s \to \infty$ is $S_{rc} = G_s w_c / e$; where, $G_s$ is soil particle specific density and $e$ is void ratio. Using $S_{rf}^*$ obtained in this way, the dehydration curve can be expressed by the following equation.

$$S_r = \frac{S_{rf}^* - S_{rc}}{1 + \exp\left(A^D + B^D \log_e s_1\right)} + S_{rc} \tag{7}$$

Where, $S_e$ is the effective degree of saturation; $S_r$

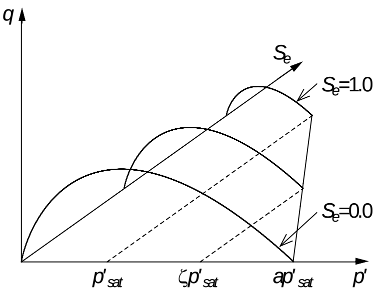


Fig.1 Conceptual diagram of the yield surface of unsaturated soil

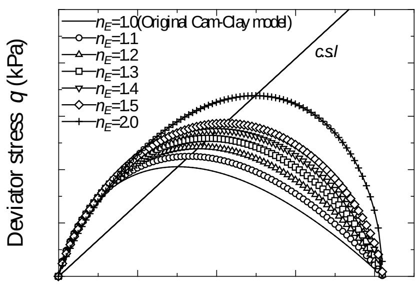


Fig.2 Yield surface of the EC model

is the degree of saturation; $s$ is the suction; $S_{rc}$ is the degree of saturation at $s \to \infty$ ; $S_{rf}$ is the degree of saturation in $s = 0$ ; and $A, B$ are fitting parameters of moisture characteristics (subscript $D$ indicates dehydration).

The water absorption curve that passes through an arbitrary suction-saturation degree ($s_1$ , $S_{r1}$) has a non-constant convergence saturation at $s \to \infty$, so unlike the dehydration curve, two parameters $S_{ra}$ and $S_{rf}$ must be determined. In other words, it is sufficient to find $S_{ra}^*$ that satisfies the following equation:

$$\frac{S_{r1} - S_{ra}}{S_{rf}\left(S_{ra}^*\right) - S_{ra}^*} = \frac{1}{1 + \exp\left(A^W + B^W \log_e s_1\right)} \tag{8}$$

This yields the dehydration curv

### 3.3 Formulation of The Finite Element Method

The governing equation in the unsaturated soil/water /air coupled problem consists of a balanced ceremony, an effective stress formula, an unsaturated elastic-plastic constitutive equation, a conformity expression, Darcy's rule, air Darcy's rule, a continuous conditional expression, and a continuous conditional expression considering gas phase, and is given by the following equations.

・Balanced ceremony

$$\mathrm{div}\boldsymbol{\sigma}^T + \rho\mathbf{g} = 0, \quad \boldsymbol{\sigma} = \boldsymbol{\sigma}^T \tag{9}$$

・Effective stress formula

$$\boldsymbol{\sigma}' = \boldsymbol{\sigma}^N + p_s\mathbf{1}, \quad \boldsymbol{\sigma}^N = \boldsymbol{\sigma} - p_a\mathbf{1} \tag{10}$$

・Unsaturated elastic-plastic constitutive equation

$$\dot{\boldsymbol{\sigma}}' = \mathbf{D} : \dot{\boldsymbol{\varepsilon}} - \mathbf{C}^S \dot{S}_e \tag{11}$$

・Conformity expression

$$\boldsymbol{\varepsilon} = -\frac{1}{2}(\nabla\mathbf{u})^S \tag{12}$$

・Darcy's rule

$$\tilde{\mathbf{v}} = -\mathbf{k} \cdot \mathrm{grad}h \tag{13}$$

・Air Darcy's rule

$$\tilde{\mathbf{v}}_a = -\mathbf{k}_a \cdot \mathrm{grad}p_a \tag{14}$$

・Continuous conditional expression

$$n\dot{S}_r - S_r\dot{\varepsilon}_v + \mathrm{div}\tilde{\mathbf{v}} = 0 \tag{15}$$

・Continuous conditional expression considering gas phase

$$(1 - S_r)\dot{\varepsilon}_v + n\dot{S}_r - n(1 - S_r)\frac{\dot{p}_a}{K_a} - \mathrm{div}\tilde{\mathbf{v}}_a = 0 \tag{16}$$

Where, assuming that saturation is a function that can be expressed only by suction, the following equation is obtained.

$$\dot{S}_r = \frac{dS_r}{ds}\dot{s} = -\frac{dS_r}{ds}\dot{p}_w \tag{17}$$

In addition, the increment of suction stress in Equation (10) is calculated by the following equation.

$$\begin{aligned} \dot{p}_s &= \frac{\dot{S}_r}{1 - S_{rc}}s + \frac{S_r - S_{rc}}{1 - S_{rc}}\dot{s} \\ &= \frac{1}{1 - S_{rc}}\left(\frac{dS_r}{ds}s + S_r - S_{rc}\right)\dot{s} \end{aligned} \tag{18}$$

Furthermore, $S_{rc}$ is the saturation degree indicated by the adsorbed aqueous phase and is a material constant.

Here, $\boldsymbol{\sigma}'$ is the effective stress tensor; $\boldsymbol{\sigma}^N$ is the base stress tensor; $\boldsymbol{\sigma}$ is the total stress tensor; $p_s$ is the suction stress; $p_a$ is the pore air pressure; $\mathbf{D}$ is the elastic stiffness tensor; $\boldsymbol{\varepsilon}$ is the strain tensor; $\mathbf{C}^S$ is the coefficient tensor; $S_e$ is the effective degree of saturation; $\mathbf{u}$ is the displacement vector; $\tilde{\mathbf{v}}$ is the flow velocity vector of interstitial water; $\mathbf{k}$ is the permeability coefficient tensor; $h$ is the all head; $S_r$ is the degree of saturation; $\varepsilon_v$ is the volumetric strain; $n$ is the porosity; $K_a$ is the air pressure; $\tilde{\mathbf{v}}_a$ is the flow velocity vector of interstitial air; and the superscript $S$ indicates the symmetric part of the tensor in ( ).

## 4. COMPACTION BEHAVIOR CONSIDERING SOIL MATERIAL

### 4.1 Analysis Conditions

In this study, the coupled soil/water/air finite element analysis program (DACSAR-MP) was used to analyze static compaction tests considering material properties.

As shown in Fig.3, a specimen of 5 cm in length and 5 cm in width was assumed for the analysis domain. To make it easier to see the flow of water, the specimen was made slightly smaller than a normal specimen. This specimen was divided into 10 elements.

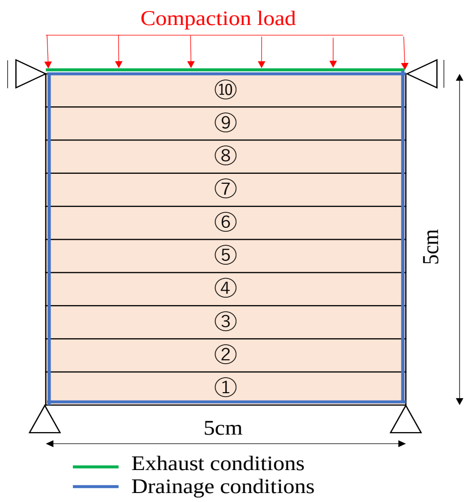


Fig.3 Finite element analysis model

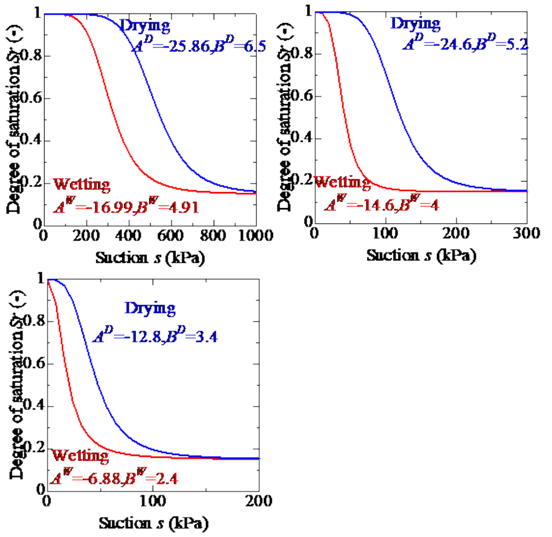


Fig.4 Water retention curve (upper left: clay, upper right: silt-mixed sand, lower left: sand)

Table 1. Material parameters (first row: clay, second row: silt-mixed sand, third row: sand)

| $\lambda$ | $\kappa$ | $M$ | $\nu'$ | Ka(m/min) | Kw (m/min) | $G_s$ | $m$ |
|---|---|---|---|---|---|---|---|
| 0.19 | 0.019 | 1.33 | 0.33 | $6.0\times10^{-9}$ | $6.0\times10^{-7}$ | 2.70 | 0.8 |
| $a$ | $n$ | $e_0$ | $\gamma_t$ | $S_{r0}$ | $n_E$ | $m$(subloading surface) | $P'_{sat}$ |
| 10.0 | 1.0 | 0.9 | 1.5 | 0.15 | 1.3 | 10 | 15.0 |

| $\lambda$ | $\kappa$ | $M$ | $\nu'$ | Ka(m/min) | Kw (m/min) | $G_s$ | $m$ |
|---|---|---|---|---|---|---|---|
| 0.14 | 0.016 | 1.33 | 0.33 | $6.0\times10^{-4}$ | $6.0\times10^{-4}$ | 2.70 | 0.8 |
| $a$ | $n$ | $e_0$ | $\gamma_t$ | $S_{r0}$ | $n_E$ | $m$(subloading surface) | $P'_{sat}$ |
| 10.0 | 1.0 | 0.9 | 1.709 | 0.15 | 1.3 | 10 | 8.0 |

| $\lambda$ | $\kappa$ | $M$ | $\nu$ | Ka(m/min) | Kw (m/min) | $G_s$ | $m$ |
|---|---|---|---|---|---|---|---|
| 0.11 | 0.011 | 1.33 | 0.33 | $6.0\times10^{-3}$ | $6.0\times10^{-3}$ | 2.70 | 0.6 |
| $a$ | $n$ | $e_0$ | $\gamma_t$ | $S_{r0}$ | $n_E$ | $m$(subloading surface) | $P'_{sat}$ |
| 5.0 | 1.0 | 0.8 | 1.8 | 0.15 | 1.3 | 10 | 8.0 |

**[Boundary conditions]**

<The displacement boundary>

・Lower side: x, y-axis fixed
  Right left side: x-axis fixed

<The air boundary>

・Upper side: exhaust conditions

・Lower side, right left side: non-exhaust conditions

<The head boundary>

・Totally undrained

**[Initial conditions]**

・ Initial moisture content: w=6%~32% (1%~2% increments)

・Loading load: 100 kPa to 100 kPa increments

・Loading time: 50 min

・Unloading time: 5 min

The material constants used in the analysis are shown in Table 1 for the three cases of clay, silt-mixed sand, and sand, respectively. The moisture property curves are shown in Fig. 4.

Here, regarding the material parameters, $\lambda$ is the expansion index; $\kappa$ is the compression index; M is the limit state parameter; $\nu$ is the Poisson's ratio; $k_a$ is permeability [m/day]; $k_w$ is saturated hydraulic conductivity [m/day]; $G_s$ is the soil particle density; m is the unsaturated permeability coefficient of Mualem [9]; a is a magnification parameter of consolidation yield stress by unsaturation; n is the $E_c$ model parameter; $e_0$ is the initial void ratio; $\gamma_t$ is wet unit volume weight; $S_{r0}$ is the critical saturation; $n_E$ is the enlargement ratio of yield surface; $m$ is the subloading surface parameter; and $p'_{sat}$ is consolidation yield stress due to unsaturation.

### 4.2 Analysis Results and Discussion

Fig. 5 shows the compaction curves for each material obtained from the displacement of the contact point of the uppermost element in the analysis domain shown in Fig. 4. The analysis was terminated at the load at which the pore pressure turned positive and the compacted soil was confirmed to be in a leaky condition (1100 kPa for clay, 700 kPa for silt mixed sand, and 700 kPa for sand). As similarly demonstrated by Kawai et al, all of the compaction curves obtained were convex upward along the zero-air gap curve from the elastic region to the plastic region as the water content increased from low to high, in line with the laboratory test results. Furthermore, by using a subloading surface model, a smooth compaction curve could be expressed.

Using the quantities obtained from the compaction curves, a mechanical interpretation of the compaction mechanism was attempted. Fig. 6 shows the results of various characteristics for each material at 1000 kPa for clay and 600 kPa for silt-mixed sand and sand. The obtained optimum moisture content ratio was compared with the results at 2% before and after the optimum moisture content ratio was reached. The dry side, the optimum moisture content ratio, and the wet side are black, red, and blue lines, respectively.

First, we examine the change in pore water pressure over time. For each material, the pore water pressure remained negative at the optimum water content and at relatively drier water contents. On the other hand, the pore water pressure turned to positive pressure at the relatively wetter side of the optimum water content ratio. Pore water pressure turned positive at the optimum water content ratio when the load was 1100 kPa for clay and 700 kPa for silt-mixed sand and sand. The fact that the pore water pressure turned positive indicates that the compacted soil was in a leaky state; the boundary conditions for compaction were not satisfied; and the compaction

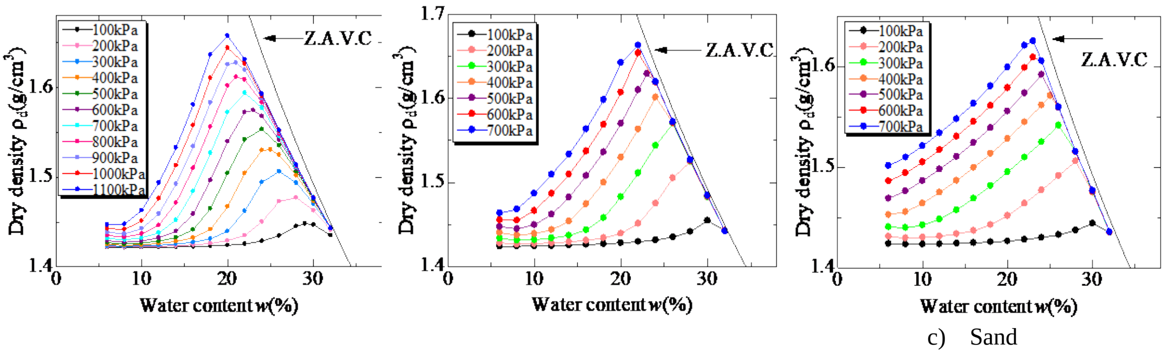


Fig.5 Compaction curves

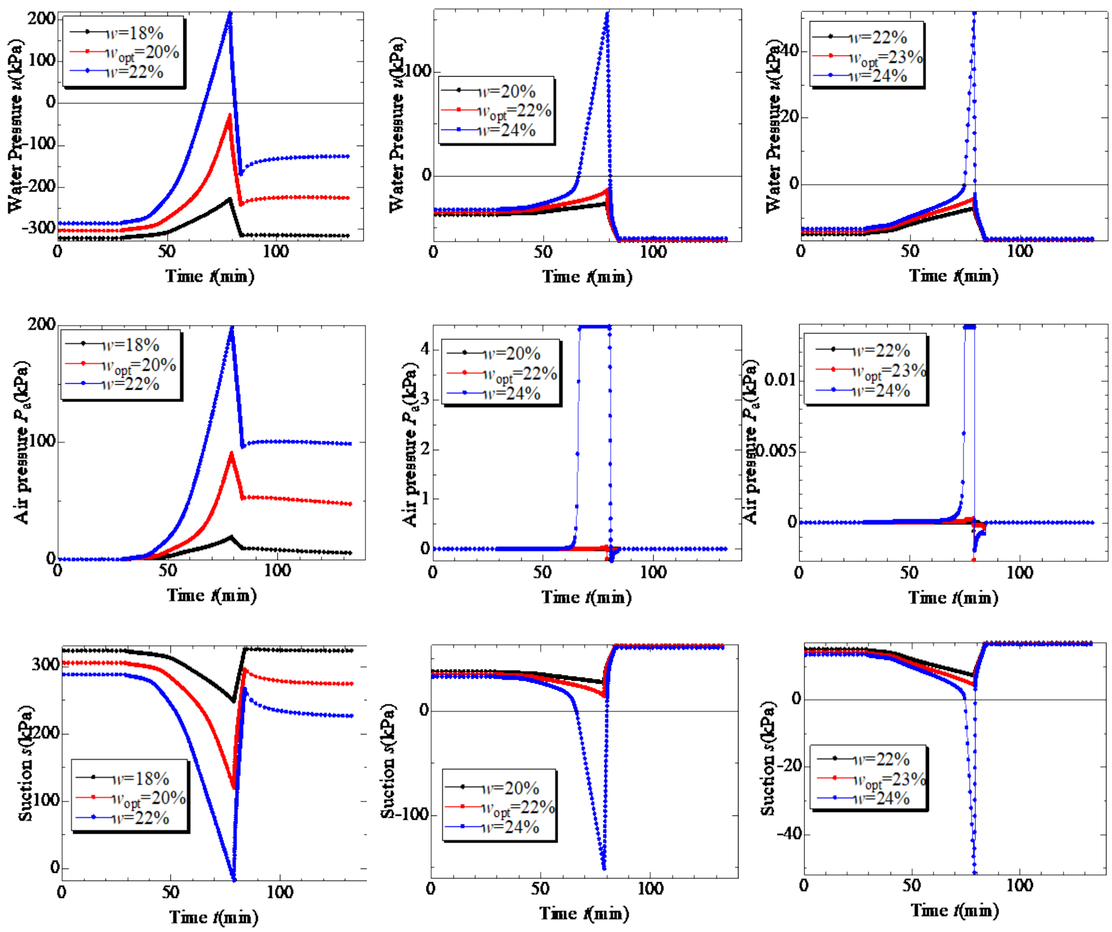


Fig. 6 Chronological change for each parameter

effect was not achieved.

Next, we examine the change in pore air pressure over time. The pore air pressure of clay remained high after unloading, while that of silt-mixed sand and sand showed almost no change from pre-loading conditions. This indicates that the effect of pore pressure is not caused by suction in silt-mixed sand and sand. In the case of clay, the air inside the soil is not fully released due to the characteristics of the material, indicating that the compaction effect is not sufficiently effective.

Finally, we examine the change in suction over time. The suction expression at unloading was significantly different between the relatively drier side and the wetter side of the optimum moisture content ratio. On the wetter side, the change in suction during unloading was large, and suction dropped to a negative value. This phenomenon occurred even at the optimum water content ratio, at 700 kPa for silt-mixed sand and sand. In the case of clay, pore air pressure also plays a role in suction development, so suction was positive even at a loading of 1100 kPa. However, the pore water pressure also turned positive, indicating that the compaction effect was not achieved.

In the compaction curves shown in Fig.5, the

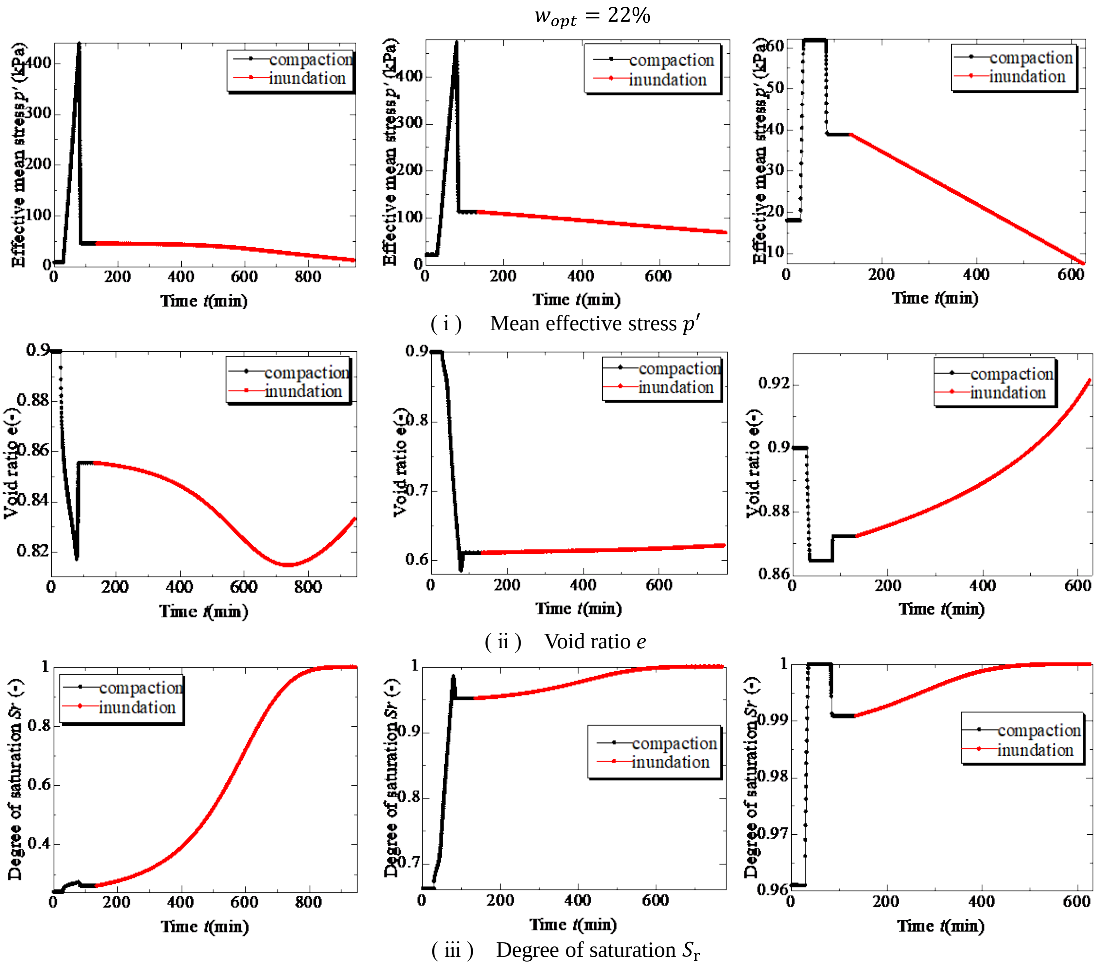


Fig. 7 Chronological change for each parameter

optimum water content ratio did not change at 1000 kPa and 1100 kPa for cohesive soil and at 600 kPa and 700 kPa for silt-mixed sand and sand. The fact that the optimum water content ratio did not change even when the load was increased indicates that the compaction effect was not obtained.

The suction effect (pore pressure) results and the compaction curves show that water leaked during compaction at 1100 kPa for clay and at 700 kPa for silt-mixed sand and sand, and that there was no change in optimum water content. This suggests that the specimens were over-compacted as they approached the saturated state from the unsaturated state, even though the compaction curve could still be drawn. Therefore, the analysis shows that the maximum compaction load that can achieve the best compaction effect is 1000 kPa for cohesive soils and 600 kPa for silt-mixed sand and sand.

## 5. INUNDATION ANALYSIS

To understand the collapse phenomenon associated with water absorption in unsaturated soils, this study performed a flooding analysis and compared the results after inundation with the initial water content ratio (initial saturation) as an internal condition to understand the soil's mechanical behavior.

### 5.1 Analysis Method

The maximum compaction load of 600 kPa for the silt-mixed sand obtained from the compaction analysis was used to represent the flooding collapse of the specimen by increasing the water head from the bottom surface after compaction. The optimum moisture content and maximum dry density of the specimens were 22% and 1.65 g/cm3, respectively. The initial water content ratios were 8%, 20%, 22%, 24%, and 32%.

### 5.2 Analysis Method

The results of the analysis are shown below. First, we examine changes from different initial water content ratios. Fig. 7 shows the mean effective stress *p'*, void ratio *e*, and degree of saturation $S_r$, respectively. The results of the mean effective stress p' illustrate that for all initial water content ratios, the values are lower after inundation than after compaction, indicating that strength is reduced due to water immersion. The void ratio e indicates that at low initial water content, the void ratio is smaller than after compaction, indicating compressive behavior. At the optimum water content, the void ratio did not change much. Swelling behavior was predominant at high water content. In addition, examining the degree of saturation, Sr, confirms that at higher water contents, i.e., water contents that show swelling behavior, transitions from an unsaturated to saturated state during compaction indicate that the initial degree of saturation influences the deformation after compaction.

These results indicate that the responses to the water table are divided into two groups: one on the compaction side and the other on the swelling side, depending on the initial water content (initial saturation) during the rise of the water table. In the case of low water content, the behavior is mainly compressive, and the pore ratio decreases despite the lower effective stress. This indicates the occurrence of internal fractures(collapses) peculiar to unsaturation.

## 6. CONSTANT VOLUME SHEAR ANALYSIS

In addition to inundation as an external factor, it is also important to understand strength properties due to shear for the stability analysis of unsaturated soils. In the case of unsaturated soil, the influence of other factors, such as the magnitude of suction in the soil, exhaust and drainage conditions, and other characteristics, are considered. In this study, compaction was considered as an unsaturated exhaust and undrained compressive deformation, and constant volume shear was applied to a specimen of silt-mixed sand under undrained conditions to analytically investigate strength properties.

### 6.1 Analysis Method

The material parameters, moisture property curves, and analysis domain used were the same as in the previous section, using silt-mixed sand. After compaction, the specimens were subjected to constant volume shear by applying strain until failure.

### 6.2 Analysis Results

Fig. 8shows the stress paths in the compaction and shear processes. The black line represents the behavior due to compaction and the red line represents the behavior due to shear. It can be seen analytically that the compaction causes the yield surface to expand, and the shear process causes it to hit the limit state line, leading to failure. Fig. 9 shows the maximum shear strength at each water content ratio. Here, it can be seen that the shear strength increases gradually from the low water content ratio toward the optimum water content ratio, but decreases abruptly when the optimum water content ratio is exceeded. These results are consistent with the shear behavior shown by Farzad et al[10]. to decrease with increasing initial water content, confirming the consistency of the analysis. Since there is no significant difference in suction change before and after the optimum moisture content ratio, it is necessary to investigate this factor in the future. However, in the present analysis, the strength was shown to be dangerous because it resulted in a significant decrease in strength on the wet side above the optimum moisture content ratio.

These results are consistent with the results proposed by Sakamoto et al[11] that more strength and stiffness can be expected in the dry side of the water content range and with the deformation and strength properties of compacted soil in shear proposed by Kawajiri et al[12], and confirm the validity of the analysis.

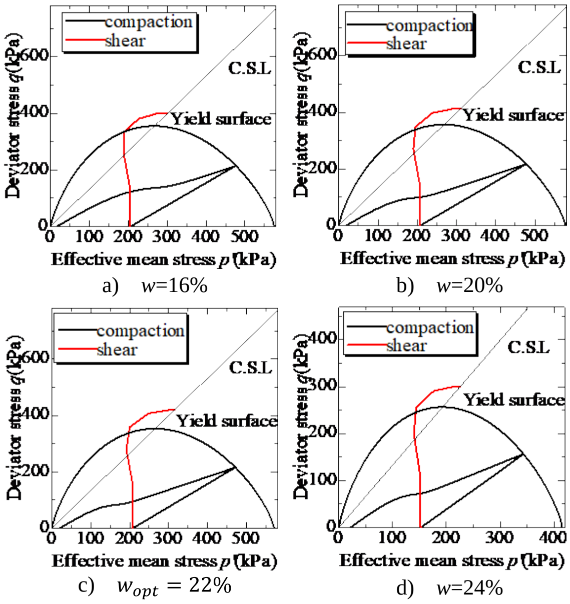


Fig. 8 Stress path

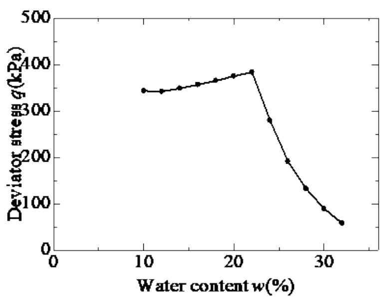


Fig. 9 Relation between water content and shear strength

## 7. CONCLUSION

The compaction analysis analytically identified over-compaction pressure.
In the water inundation analysis, the threshold of collapses was determined, and it was confirmed that

the embankment exhibited strength on the drier side than the optimum water content ratio.

The shear analysis also showed that strength was exhibited on the dry side, indicating that construction on the dry side would result in a stronger embankment. The results of this analysis are close to those of the actual conditions and can be applied to a variety of materials and conditions.

## 8. REFERENCES


[1] Kanazawa S., Toyoshima K., Kawai K., Tachibana S. and Iizuka A.: Analysis of mechanical behavior of compacted soil with F.E. method, journal of JSCE, No.68 (2), pp.291-298, 2012.

[2] Kawai K., Shibata M., Kanazawa S.: Simulations of static compaction with unsaturated soil/water coupled F.E. code, journal of JSCE, No,12, pp.429-436, 2009.

[3] Ohno S., Kawai K. and Tachibana S.: Elastic-plastic constitutive model for unsaturated soil applied effective degree of saturation as a parameter expressing stiffness, journal of JSCE, Vol.63/No.4, pp.1132-1141, 2007.

[4] Karube D., Kato S., Hamada K. and Honda M.: The relationship between the mechanical behavior and the state of porewater in unsaturated soil, journal of JSCE, No.535/III-34, pp.83-92, 1996.

[5] Ohno S., Iizuka A. and Ohta H., Two categories of new constitutive model derived from non-linear description of soil contractancy, Journal of applied mechanics, pp. 407-414, 2006.

[6] Schofield, A and Wroth, P. : Critical State Soil Mechanics, McGraw-Hill, pp. 1-310, 1968.

[7] Roscoe, K. H and Burland, J. B.: On the Generalised stress-Strain behavior of wet clay, engineering plasticity eds. J. Heyman and F. A. Leckie, Cambridge University Press, pp.535-609, 1968.

[8] Awal A.S.M.A, Hosseini H. and Hossain M.Z., Strength, Modulus of Elasticity and Shrinkage Behaviour of Concrete Containing Waste Carpet Fiber, International Journal of GEOMATE, Vol. 9, Issue 17, 2015, pp. 1441-1446.

[9] Farzad H., Hamid N.: Characterisation of the undrained shear strength of expansive clays at high initial water content using intrinsic concept, International Journal of GEOMATE, 2018, Vol.14, Issue 44, pp.176-182.

[10] Sakamoto H., Tatsuoka H., Soda H., Kobayashi H. and Obara T.: Soil compaction method based on the control of compaction energy and saturation degree for impermeable embankment, journal of JSCE, No,1, pp.43-58, 2021.

[11] Shunzo Kawajiri., Takayuki Kawaguchi., Shintaro Yamasaki., Dai Nakamura., Satoshi Yamashita1 and Satoru Shibuya.: Strength characteristics of compacted soil with particular reference to soil structure and anisotropy, International Journal of GEOMATE, Oct., 2017, Vol.13, Issue 38, pp.178-185